October 29, 2003

Ken Zweibel
National Renewable Energy Laboratory
1617 Cole Boulevard
Golden, CO 80401

Re: NREL Subcontract #ADJ-1-30630-12

Dear Ken:

This report covers research conducted at the Institute of Energy Conversion (IEC) for the period, Sept. 10, 2003 to Oct. 09, 2003, under the subject subcontract. The report highlights progress and results obtained under Task 2 ($CuInSe_2$-based Solar Cells).

Task 2: $CuInSe_2$-based Solar Cells

In-line Evaporation

The main effort during the present period was concentrated on modifying the Se sparger system, providing Se flux onto the substrate. The system consists of a source bottle heated by an electrical heater, a main manifold and four branches with two effusion holes each (Figure 1.) along the sides of the Cu, Ga and In sources.

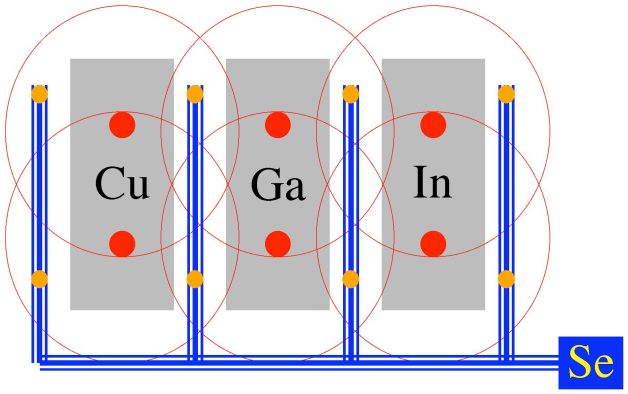

Fig 1. Source layout in the CIGS in-line deposition system.

The primary issue was the control of the surface temperature of the Se melt in the source bottle. Since Se source receives substantial amount of heat from Cu, Ga and In sources a heat shield was installed between these sources and the Se bottle. There is, however, heat coming into the Se bottle by conduction from the manifold. This heat source along with the spiral electric heater placed towards the top of the Se bottle, create a temperature gradient in the Se source. Se temperature is the highest at the top where the manifold is attached, and the coldest at the bottom of the source. Under these circumstances, as Se is used up, the level goes down; and since the control thermocouple immersed into the melt is stationary, it indicates the true surface temperature only when the melt level is at the same level as the thermocouple tip. This problem was solved by using a 0.01" OD inconel sheeted thermocouple, attached to a graphite ring, placed inside the source with a certain amount of slack on the thermocouple. During the operation, the graphite ring floats over the melt; and since the thermocouple is thin, as the melt level changes graphite ring stays floating over the melt and the thermocouple always give the surface temperature as long as there is source material in the bottle.

Another problem with controlling Se flux onto the substrate was that Se was found to condense in the branches during start-up and/or cool-down creating secondary uncontrolled sources. This problem was solved by carefully monitoring the temperature of all the source shields, Se branches and Se source bottle and making sure that branches between the metal sources is always hotter than the Se source. Under these circumstances Se will always condense into the source not in the branches. This was achieved by properly sequencing the temperatures during heat-up and cool-down. Figure 2 shows the relevant temperatures during a run, as a function of temperature, in which the proper sequencing allowed the Se source to be the coolest point at all times. The efficacy of this scheme was verified by depositing just Cu right after a CIGS deposition. There was no selenide in the resulting film indicating that no condensation was present in the Se branches.

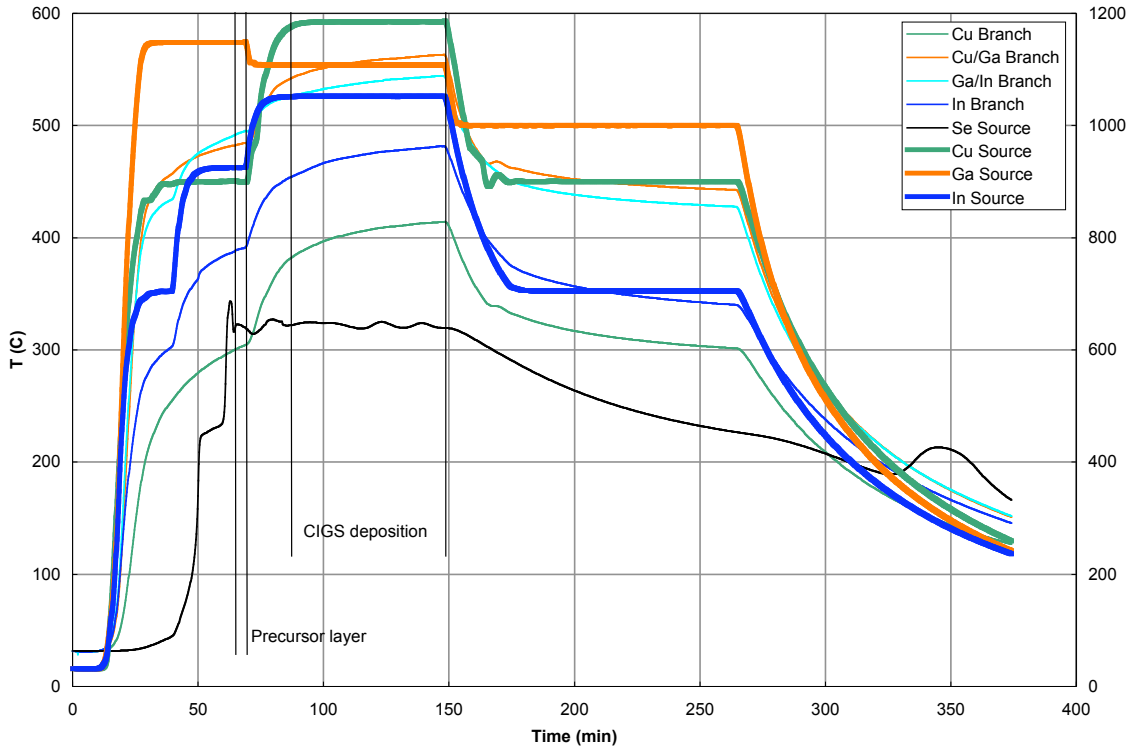

Fig. 2. Temperature of the sources and of the Se branches during a CIGS run where heaters were properly sequenced during heat-up and cool-down to keep Se source temperature the lowest. Right hand scale shows temperature of the Cu, Ga and In sources.

Wide Bandgap Materials

S-diffusion in $Cu(InGa)Se_2$

Efforts continued to develop a quantitative understanding of the diffusion of S into $CuInSe_2$ thin films during post-deposition sulfurization. As shown in the previous report under this contract, the lattice diffusion coefficient D_l was determined to be a function of the concentration $y \equiv S/(Se+S)$ by analyzing diffusion profiles of S into $CuInSe_2$ single crystals using a Boltzmann-Matano method. The grain boundary diffusion coefficient D_b in polycrystalline films can be determined using D_l. However, this will require smooth films, in order to justify the model assumptions about the diffusion geometry and the measurement procedure. Films grown in a two-step co-evaporation process at IEC have surface roughness rms values in the range of 300 to 400□m, according to AFM data. In contrast, the polished crystals had rms roughness <10□m. Two approaches are being pursued to prepare similarly smooth films for sulfurization experiments, without damage to the film structure. One is the removal of films from their substrate with a high-temperature epoxy, in order to expose the smooth back surface of the film for sulfurization. Different epoxies are being evaluated to find one which can withstand the

conditions needed for the sulfur reactions done in flowing H_2S at up to 575°C. Alternatively, films are being chemo-mechanically etched with a lapping cloth wetted with an oxidizing agent, so that the film surface is oxidized and the cloth mechanically removes the oxides. The procedure is completed by an etch that removes remaining oxides. The smoothed films will be reacted in H_2S and AES depth profiles, which will be measured. The resulting data will be analyzed with the help of the thin-film diffusion model, allowing for the determination of the values of D_l and D_b.

Fundamental Materials and Interface Characterization

Cu(InGa)Se_2 Optical Characterization

A paper titled "Optical characterization of CuIn1-xGaxSe$_2$ alloy thin films by spectroscopic ellipsometry" by P. D. Paulson, R. W. Birkmire, and W. N. Shafarman was published in the Journal of Applied Physics [i]. In this work, optical constants of polycrystalline thin film $CuIn_{1-x}Ga_xSe_2$ alloys with Ga/(Ga+In) ratios from 0 to 1 were determined by spectroscopic ellipsometry over an energy range from 0.75 to 4.6eV. $CuIn_{1-x}Ga_xSe_2$ films were deposited by simultaneous thermal evaporation of elemental copper, indium, gallium and selenium. X-ray diffraction measurements showed that the $CuIn_{1-x}Ga_xSe_2$ films were single phase. Due to their high surface roughness, the films were generally not suitable for ellipsometer measurements. An innovative method was developed in which spectroscopic ellipsometer measurements were carried out on the reverse side of the $CuIn_{1-x}Ga_xSe_2$ films immediately after peeling them from the Mo-coated soda lime glass substrates. A detailed description of multilayer optical modeling of ellipsometric data, generic to ternary chalcopyrite films, was presented and used to obtain accurate values of the refractive index (n) and extinction coefficient (k). An extensive table listing n and k with Ga/(In+Ga) = 0, 0.31, 0.45, 0.66 and 1 over the energy range $0.75 \leq E \leq 4.6$ eV was included. The effects of varying Ga concentration on the electronic transitions were are shown for the fundamental transitions $E_0(A)$, $E_0(B)$ and $E_0(C)$ in Figure 1. For the bandgap Eg, this data gives a bowing parameter b = 0.26.

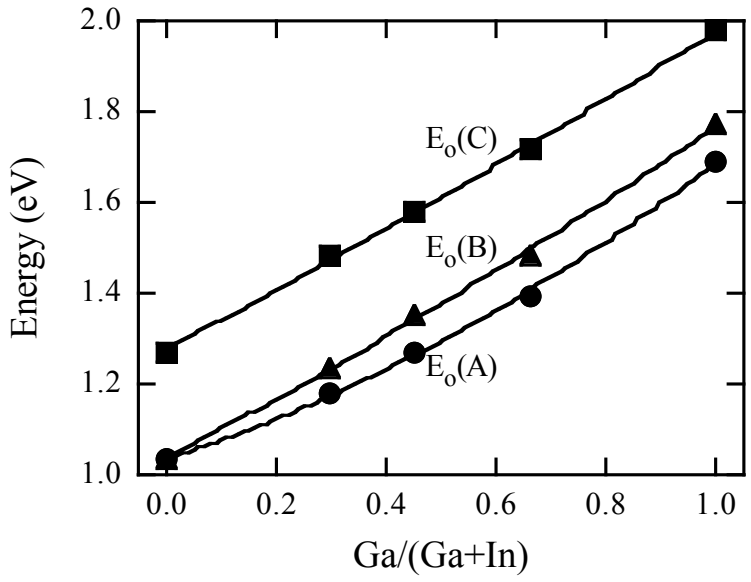

Figure 1. Variation in the fundamental absorption transitions $E_0(A)$, $E_0(B)$ and $E_0(C)$ of $CuIn_{1-x}Ga_xSe_2$ films with x.

Mo/$CuInSe_2$ Interface Characterization

The Mo/$CuInSe_2$-alloy interface is being characterized with the goal of understanding the fundamental characteristics that control adhesion and affect device performance. We have previously identified poor adhesion at the Mo interface as a critical issue in the fabrication of cells using inline evaporation of Cu(InGa)Se_2 on flexible polyimide substrates [ii] and using Cu(InAl)Se_2 absorber layers [iii]. In each case, the adhesion was improved by the deposition of excess Ga at the Mo interface.

The present effort is focused on formation of a $MoSe_2$ interfacial layer during the $CuInSe_2$-alloy deposition [iv]. The role of $MoSe_2$ in Cu(InGa)Se_2 devices is not well understood, even though it plays a role in the formation of ohmic contact between Mo and Cu(InGa)Se_2. However, $MoSe_2$ has a layered structure, similar to mica, in which planes with Se-Se bonds can be easily cleaved leading to adhesion problems. TEM studies by Nishiwaki et. al. [iv] showed that the orientation of the $MoSe_2$ plays an important role in controlling the adhesion properties. Adhesion is best with the $MoSe_2$ c-axis parallel to the Mo layer so the Se-Se planes are perpendicular to the substrate. In this case, an XRD pattern will show (100) and (110) diffraction peaks. Delamination is more likely with the Se-Se planes parallel to the substrate, in which case, (002) diffraction peaks will be observed. Thus, a specific objective of this work is to determine how Ga and/or Al at the Mo interface affects the $MoSe_2$ formation and orientation. Additional objectives include determining if growth conditions for the Mo deposition or Cu(InGa)Se_2 evaporation can control the $MoSe_2$ formation, and how it is affected by the presence of Na from the glass substrate.

Initial experiments have been done to characterize the formation of $MoSe_2$ by reaction of Mo layers, deposited on either soda lime (SLG) or borosilicate glass (BSG), which is Na free, with evaporated Se. In addition, 200A thick Ga or Cu layers were deposited on Mo films prior to Se reaction, which was done at 500°C for 1 hour. Films were characterized by XRD to determine the phases formed by the selenization reaction and their orientation. XRD measurement using Bragg-Brentano geometry was carried out from 10 to 80°. This configuration enforces □-2□ symmetry, so, only lattice planes parallel to the substrate planes would satisfy the Bragg equation resulting in diffraction peaks. Glancing incidence XRD (GIXRD) measurements were done at 0.3°, 0.4°, 0.5°, 0.6°, 0.8° and 1.0° incident angles, all above the critical angle, which correspond to a sampling depth varying from 80 nm to 270 nm. In the GIXRD measurements, the incident angle is fixed and the reflections satisfying the Bragg conditions are obtained from lattice planes tilted at different angles to the sample plane. If measurements are carried out at a different incident angle, different set of lattice planes with the same spacing but tilted from the sample plane satisfy the Bragg equation. In the present set of experiments, the variation in incident angle is sufficiently small, that the same set of lattice planes satisfy the Bragg reflection conditions.

XRD and GIXRD scans are shown in Figures 2 – 7 for selenized BSG/Mo, SLG/Mo, BSG/Mo/Ga, SLG/Mo/Ga, BSG/Mo/Cu, and SLG/Mo/Cu samples. The GIXRD data is shown with increasing incident angle displaced to higher intensity. For all samples, the XRD spectra show $MoSe_2$ peaks, which are labeled by their (hkl) indices. Mo, Ga_2Se_3 and Cu_2Se_3 peaks, when observed, are labeled by their phase but not indices. The (103) peak for hexagonal $MoSe_2$ has the highest structure factor and therefore intensity in powder patterns but is absent in all the films. This is consistent with previous results reported for $MoSe_2$ films formed by selenization of Mo films [v]. Only (002) reflections, corresponding to the $MoSe_2$ layered structure parallel to the substrate plane, and (100) and (110) reflections, arising from layers perpendicular to the substrate plane, are observed.

The orientation parameter for the three $MoSe_2$ peaks was determined from the XRD peak heights using the Harris method in which a value > 1 for a given peak indicates preferred orientation compared to a random powder diffraction pattern. The results are listed in Table 1. This shows that the $MoSe_2$ films have a preferred orientation in the (110) direction, for all cases. The films with the Cu layer, on either type of glass, have a stronger relative (002) orientation than the selenized Mo or Mo/Ga layers. There were no significant differences between the BSG and SLG substrates.

The GIXRD spectra, shown at multiple angles, have much less noise since they sample a much greater volume of the phases near the surface. In general, all the diffraction peaks in the symmetric XRD spectra are also observed in the asymmetric GIXRD spectra but with different relative peak heights. For the $MoSe_2$ phase, the most significant difference is the (110)-peak height, which is the largest peak in the XRD spectra; but is much smaller in the GIXRD data. The symmetric XRD measurements indicate that (110) lattice planes lying parallel to the sample are preferred. However, the asymmetric

GIXRD measurement requires (110) planes to be tilted by ~27° from the sample planes to satisfy the Bragg reflection condition so the peak is much smaller.

Table 1 Orientation parameter for different peaks determined using the Harris method with 3 (hkl) peaks.

	Structure	P(002)	P(100)	P(110)
IE0701	7059/Mo	0.3	1.1	1.7
IE0702	7059/Mo/Ga	0.2	0.9	1.9
IE0703	7059/Mo/Cu	0.6	0.9	1.5
IE0704	SLG/Mo	0.2	1.1	1.7
IE0706	SLG/Mo/Ga	0.2	0.8	2.0
IE0708	SLG/Mo/Cu	0.6	0.7	1.6

Additional observations from the GIXRD data include:

- For the selenized Mo, the ratio of (100) / (002) peak heights increased with increasing incident angle.
- For selenized Mo/Ga films the relative (002) and (110) peak heights behave similarly to the Mo films but the (002) peak is significantly smaller, especially on the SLG substrate. Ga_2Se_3 peaks are also observed.
- For the Mo/Cu on SLG and BSG substrates, the largest $MoSe_2$ peak is the (002). The relative (002) and (100) peak heights do not change with incident angle. Instead, Cu_2Se_3 and both (002) and (100) peaks increased with incident angle.

Additional experiments underway or planned will examine the effect of Al using selenized Mo/Al/Cu layers to prevent oxidation of the Al. In addition, the $MoSe_2$ formation after $Cu(InGa)Se_2$ or $Cu(InAl)Se_2$ growth will be characterized by peeling the absorber layers off of the substrate.

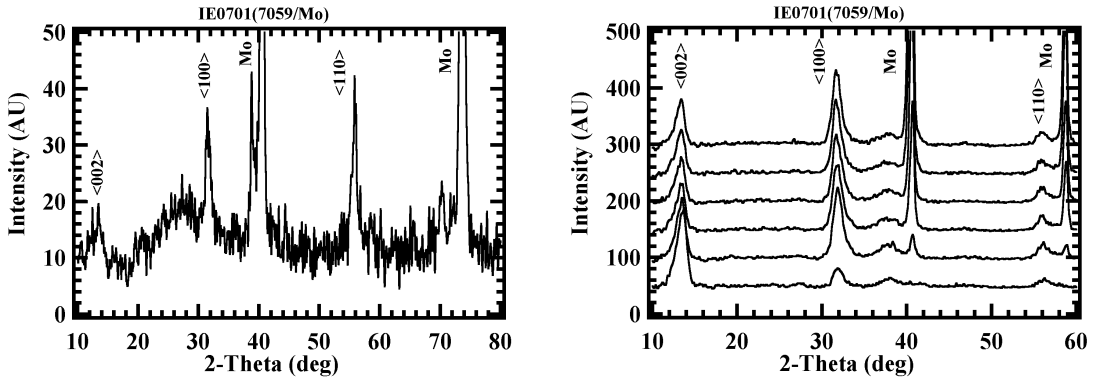

Figure 2. XRD and GIXRD spectra from selenized BSG /Mo substrates

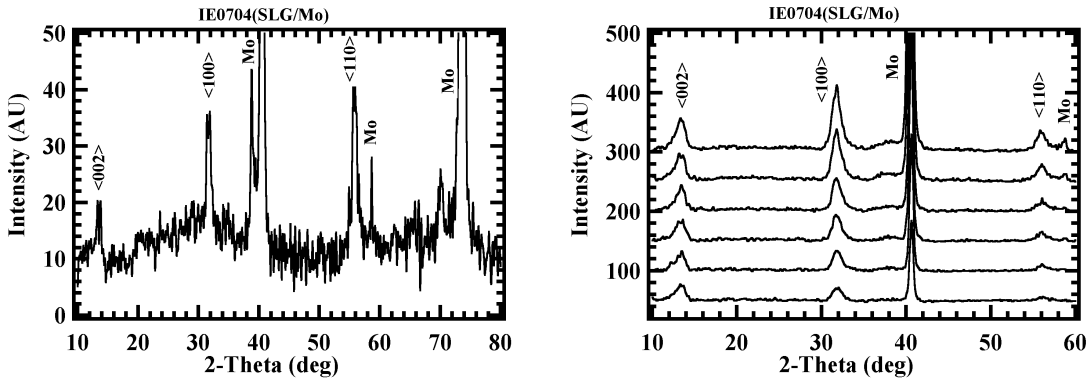

Figure 3. XRD and GIXRD spectra from selenized SLG/Mo substrates.

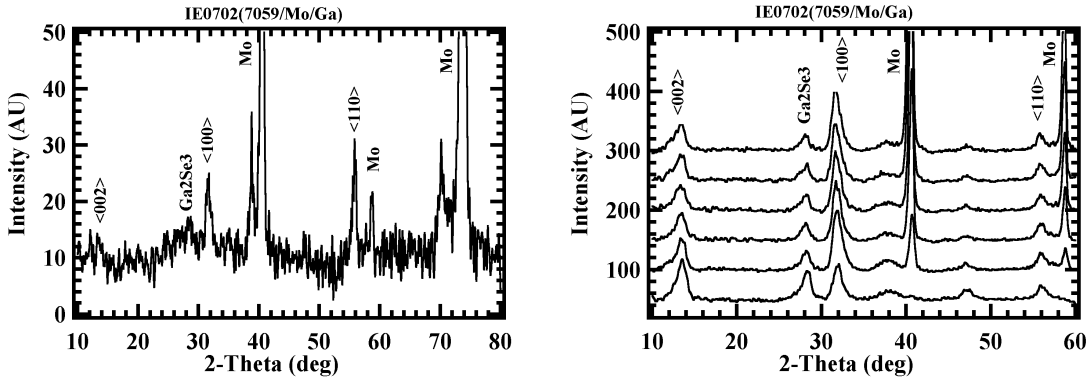

Figure 4. XRD and GIXRD spectra from selenized BSG /Mo/Ga substrates.

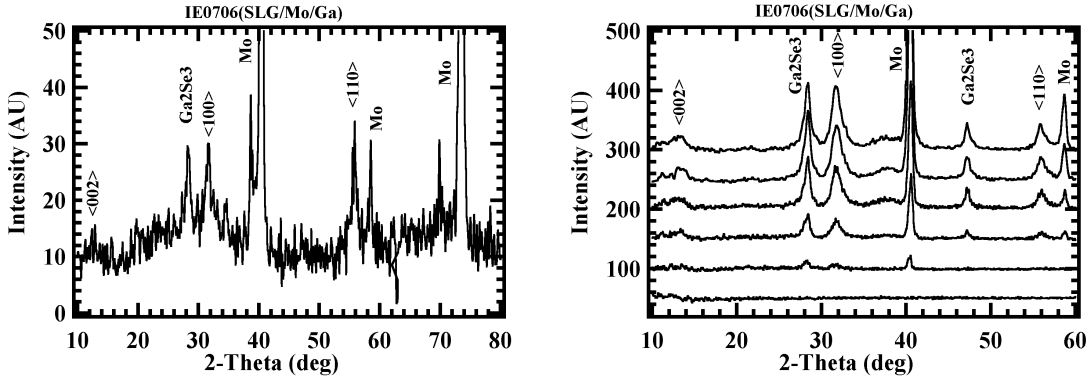

Figure 5. XRD and GIXRD spectra from selenized SLG/Mo/Ga substrates.

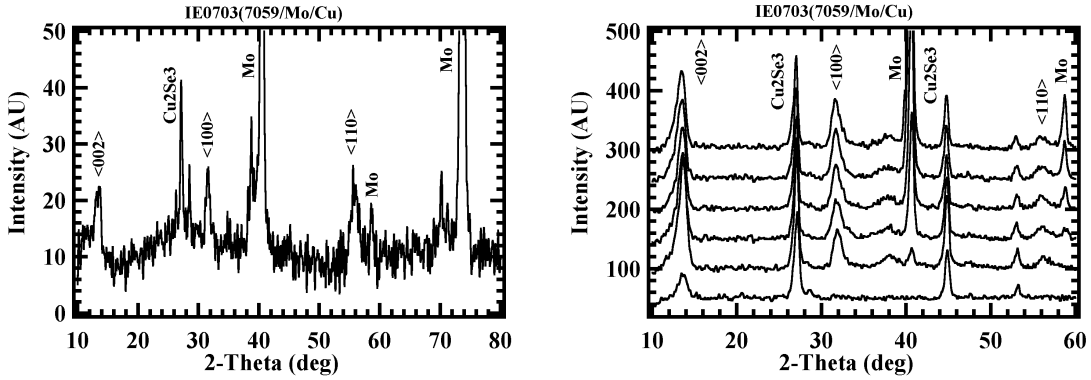

Figure 6. XRD and GIXRD spectra from selenized BSG/Mo/Cu substrates.

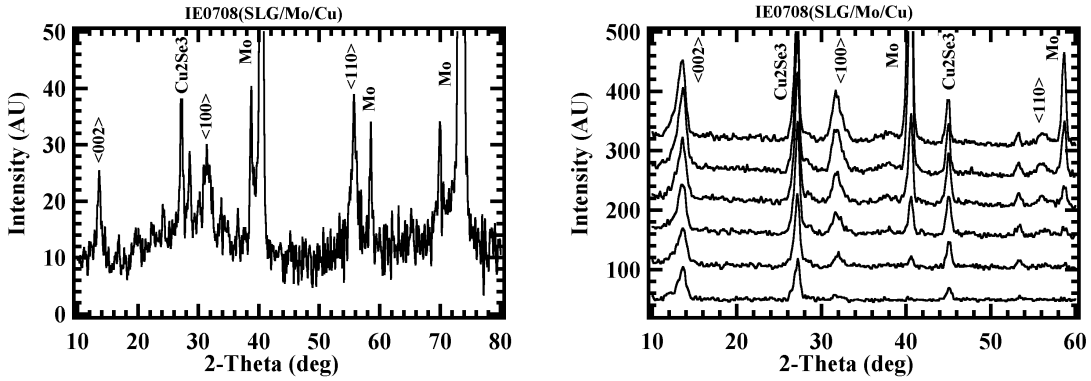

Figure 7. XRD and GIXRD spectra from selenized SLG/Mo/Cu substrates.

References

i. P.D. Paulson, R.W. Birkmire, and W.N. Shafarman, J. Appl. Phys. **94**, 879 (2003).
ii. G.M. Hanket, U.P. Singh, E.Eser, W.N. Shafarman, and R.W. Birkmire, Proc. 29th IEEE PVSC, 567 (2002).
iii. P.D. Paulson, M.W. Haimbodi, S. Marsillac, R.W. Birkmire and W.N. Shafarman, *J. Appl. Phys.* **91**, 10153 (2002).
iv. S. Nishiwaki, N. Kohara, T.Negami and T. Wada, *Jpn. J. Appl. Phys.* **37,** L71 (1998).
v. N. Kohara, S. Nishiwaki, Y. Hashimoto, T. Negami and T. Wada, *Sol. Energy. Mater & Sol. Cells.* **67,** 209 (2001).

Sincerely,

Robert W. Birkmire
Director

RWB/bj
cc: Gerri Hobbs, UD Research Office
Carolyn Lopez, NREL
Paula Newton
Erten Eser
William N. Shafarman